AMAZALERT Delivery Report

Title	Report on quantifying sensitivity of regional climate of Amazonia to feedbacks from CO_2 physiological forcing
Work Package Number	3
Delivery number	3.2
First author	Juan P. Boisier
Co-authors	Kate Halladay, Gillian Kay, Philippe Ciais and Peter Good
Date of completion	27 November 2014
Name leading Work Package Leader	Gillian Kay
Approved by the Leading Work Package Leader	Yes

Table of Contents

List of acronyms

ABG	Above Ground Biomass
C4MIP	Coupled Carbon Cycle Climate–Model Intercomparison Project
CMIP5	Coupled Model Intercomparison Project Phase 5
DGVM	Dynamic Global Vegetation Model
EMIC	Earth System Model of Intermediate Complexity
ESM	Earth System Model
GCM	Global Climate Model
LAI	Leaf Area Index
LULCC	Land Use—induced Land-Cover Change
LSM	Land Surface Model
NPP	Net Primary Production

Summary

This report presents an evaluation of the radiative and physiological effects of elevated atmospheric CO_2 concentration on the land carbon balance and climate, and of the role of Amazonian rainforest in the global changes. We analyse three idealised modelling experiences carried by eight state-of-the-arts Earth System Models (ESMs) in the context of CMIP5. These simulations serve to isolate the radiative and direct (biochemical) response to the atmospheric CO_2 change, which is prescribed to increase 1% per year starting from preindustrial conditions.

Our results reaffirm the great importance of Amazonia regarding the global feedbacks between climate and the carbon cycle. In simulations accounting for the biochemical effects of CO_2 only (i.e., no large-scale warming), this ecosystem would act as a large carbon sink; for a forcing equivalent to $3\times CO_2$, the biomass production (NPP) across Amazonia increases from around 6.6 to 10.4 PgC yr^{-1}, contributing to 13% of the global increase in vegetation carbon. However, the climate response to CO_2 that acts to reduce the uptake capacities of the biosphere globally, also affects, principally, the tropical rainforest. Accounting both for the fertilizing and the radiative effects of CO_2, the Amazon contribution to the increase in vegetation carbon stock is reduced to 9%.

The ensemble simulations assessed indicate also a significant CO_2-physiological impact on water cycle in Amazonia. The anti-transpirant effect of CO_2 reduces the basin-wide evapotranspiration by around 9%, despite the systematic increases in leaf area index (LAI). As a result, precipitation is also reduced across the basin, amplifying the drying impacts induced by the large-scale climate perturbation (radiatively-driven) at the end of the dry season. Hence, this result suggests that the precipitation response to anthropogenic forcing in Amazonia may be underestimated in climate models that do not account for biochemical processes, and could then induces biases in the assessment of the local feedbacks between vegetation and climate.

1 Introduction

The evolution of the climate system under the pressure of human activities depends on the complex interaction between the physical world and biochemical processes. The ongoing increase of the atmospheric carbon dioxide (CO_2) concentration affects the radiative properties of the atmosphere, increasing its greenhouse capacities, and leading to global warming and related changes in climate (IPCC, 2013). Yet, the change in the air CO_2 content also affects the way the biosphere and the ocean exchange gases with the environment (Ciais et al., 2013). Altogether, the vegetated lands and the ocean absorb today more than half of the atmospheric CO_2 surplus resulted from anthropogenic emissions, hence providing a fundamental ecological service (Le Quéré et al., 2014).

The capacity of the Earth to absorb part the carbon emissions is known as carbon-concentration feedback (a strong negative one in terms of atmospheric CO_2). The terrestrial contribution to this mechanism is mainly due to the enhanced plant photosynthesis with elevated ambient CO_2, and associated increase in biomass productivity and carbon store. However, in addition to this fertilizing effect, the change in atmospheric CO_2 affects the land carbon uptake indirectly through climate perturbations. Above-normal temperatures have been observed to reduce net primary productivity (NPP) (e.g., Hashimoto et al., 2004) and should increase soil respiration (Jones et al., 2003), both factors reducing the net biosphere production. The climate impact on the carbon cycle is therefore supposed to amplify the human perturbation in the future by reducing the natural carbon sink (a positive feedback; Friedlingstein et al., 2006). The climate-carbon feedbacks may constitute a big threat if other potential mechanisms, such as the partial thawing of permafrost soils (Schurr et al., 2009; MacDougall et al., 2012) or the Amazonian rainforest dieback (Cox et al., 2004), take place.

The direct effects of CO_2 on vegetation concern not only the carbon cycle and related feedbacks with the climate system, but also the surface hydrology by reducing the canopy conductance and transpiration. The Amazonian rainforest plays a major role in the regulation of both the carbon and water cycles. This ecosystem contains about half of the tropical forest and is therefore responsible for an important fraction of the global biomass production and carbon storage capacity (Field et al. 1998; Saatchi et al., 2007; Malhi et al., 2009a). An adverse climate scenario in Amazonia could trigger large impacts on the rainforest, such as the widespread dieback, with the concurrent local and global consequences. Such an extreme scenario is today very uncertain, as are the biophysical and biochemical mechanisms involved.

In this report, we evaluate the radiative and biochemical effects of CO_2 in a changing climate,

and the role of Amazonia in these processes. We present first a short review of past modelling activities accounting for the biochemical cycles and physiological effects of CO_2 (Section 2). Based on state-of-the-art ESM simulations, we then present an ongoing model intercomparison analysis of the biochemical and radiative impacts of CO_2 focused on Amazonia (Section 3). The preliminary conclusions of this study are presented at the end.

2 Background on the modelling of climate and biochemical cycles

Climate modelling is a powerful and key tool in climate research. Global atmospheric circulation models have evolved quickly to fully coupled ocean-atmosphere-land models. Recent developments include the characterization of the atmospheric chemistry and the biochemical processes on the land and ocean. Within a number of studies, this new generation of models — so-called Earth System Models (ESMs) — is used for the assessment of feedbacks between climate and biochemical cycles.

The first climate model simulations that accounted both for the carbon cycle and vegetation dynamics in an interactive way, surprised climate researchers and a wider community. The Hadley Centre climate model HadCM3(LC) indicated that the future changes in atmospheric CO_2 concentration in a pessimistic scenario of fossil-fuel emissions — and the associated impact on climate — may be substantially underestimated in GCMs (without biochemical processes) because of suppressed carbon uptake capacities of the land and the ocean in a high CO_2 world (Cox et al., 2000). An even more alarming result of these simulations was the fact that, in addition to accelerated biomass decomposition and associated enhancement of soil respiration, the climate effects on the carbon cycle is partly related to a widespread loss of rainforest in tropical South America (the so-called Amazon forest dieback, Cox et al., 2004; see Figure 1).

Further analyses indicated a drying in tropical South America as the primary cause for rainforest dieback — a feature that, although simulated in many GCMs, is of particular large amplitude in HadCM3LC (Cox et al., 2004). In this model, a significant fraction (20%) of the Amazonian rainfall reduction was attributed to the CO_2-physiological forcing (stomatal closure) and associated suppression of canopy transpiration and evapotranspiration (ET); the major cause of drying remaining the regional manifestation of the large-scale — radiative — impacts of CO_2. Decreases of precipitation initially driven by these two mechanisms are further amplified in HadCM3LC through forest loss and additional water recycling reduction (a positive feedback loop; Betts et al., 2004).

As reported in AMAZALERT Deliverable D3.4 (Kay et al., 2014), current modelling suggests that large-scale dieback driven by climate change alone by the end of the 21st century seems unlikely, in part because of the large spread of climate projections in tropical South America (Malhi et al., 2009b; Huntingford et al., 2013; Boulton et al., in prep). However, missing processes and biases (known and potential) in models are such that dieback is much harder to rule out than implied by these models alone. There are key uncertain processes, of which the role of CO_2 fertilization is one, but also include fire, drought mortality and regional rainfall dynamics, which could lead to substantial changes in model projections in the future. (Boisier et al., submitted). Further, the effects of climate variability and change combined with regional deforestation (AMAZALERT Deliverable D4.2, Aguiar et al. 2014) increases the risk of forest loss (Betts et al., 2008; Malhi et al., 2008; Nepstad et al., 2008, Marengo et al., 2009) with consequences for ecosystem service provisioning (refer to AMAZALERT Deliverable D1.2, Tejada Pinell et al., 2012, for a review of Amazon ecosystem functioning and services). The complex interaction between key local variables (e.g., rainfall regime, soil moisture, water recycling, drought, fires, tree mortality) could subject Amazonia to nonlinear outcomes, and this ecosystem has been highlighted as a possible 'tipping element' within the Earth system (see Lenton, 2011).

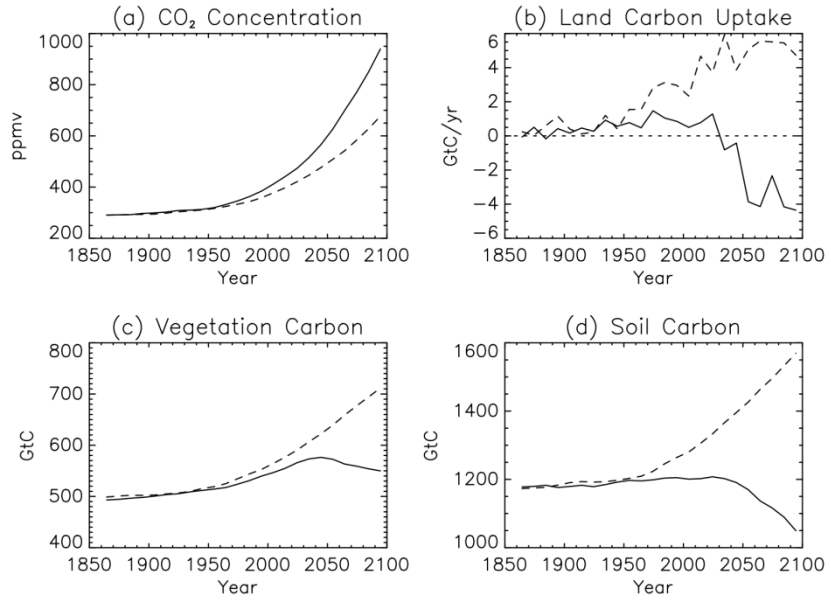

Figure 1: Impact of climate-carbon cycle feedbacks on projections of (a) atmospheric CO_2 concentration, (b) global land carbon uptake, (c) global vegetation carbon and (d) global soil carbon. The continuous line represents the fully coupled climate-carbon cycle run and the dashed line is from the run without climate effects on the carbon cycle. From Cox et al. 2004.

The coordinated evaluation of coupled climate-carbon cycle model simulations (either with ESMs or EMICs) has led to a more robust diagnosis (with estimated uncertainties) of the role of the biochemical processes in a changing climate (Figure 2). Such coordination has been systematic during the last decade, notably though the C4MIP initiative (e.g., Friedlingstein et al., 2006) and more recently through the intercomparison of CMIP5 ESMs (e.g., Arora et al., 2013; Ciais et al., 2013).

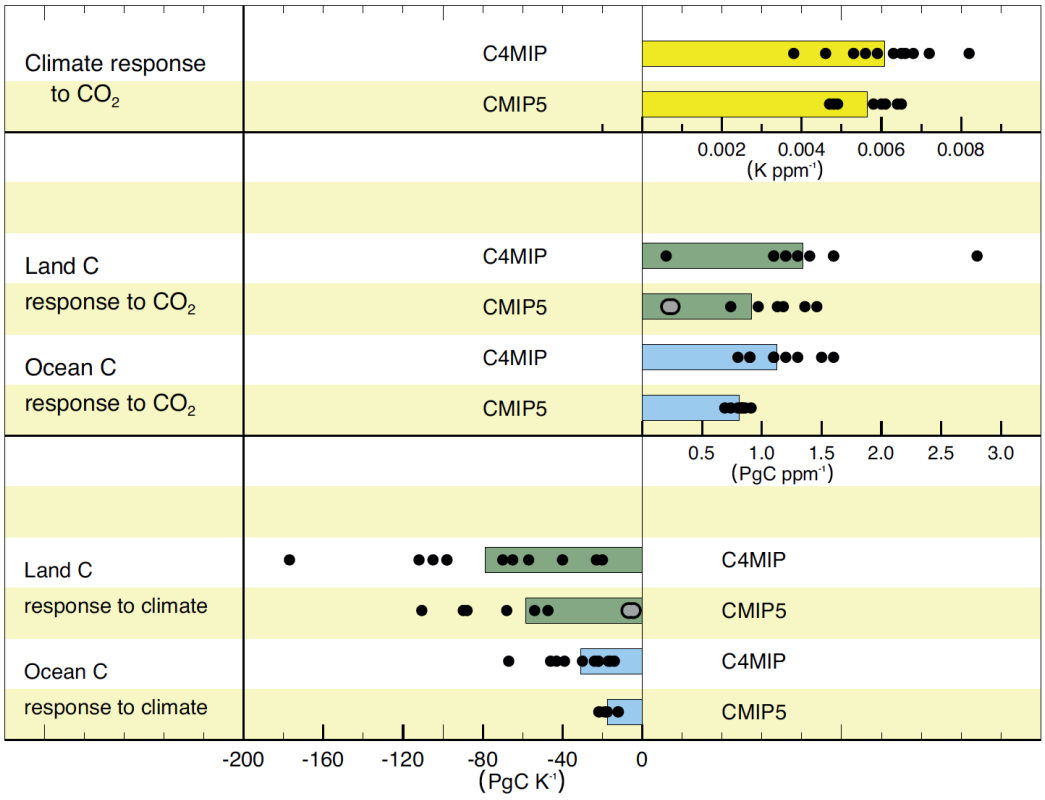

Figure 2: Comparison of carbon cycle feedback metrics between the C4MIP ensemble of seven GCMs and four EMICs under the Special Report on Emission Scenario-A2 (SRES-A2) (Friedlingstein et al., 2006) and the eight CMIP5 models (Arora et al., 2013) under the 140-year 1% CO_2 increase per year scenario. Black dots represent a single model simulation and coloured bars the mean of the multi-model results; grey dots are used for models with a coupled terrestrial nitrogen cycle. Adapted from Ciais et al., 2013.

The C4MIP and CMIP5 activities have focused, principally, on the global-scale interaction between the carbon cycle and climate, notably on the quantification of the carbon-concentration and climate-carbon feedbacks (Friedlingstein et al., 2003, 2006, 2014; Arneth et al., 2010; Arora et al., 2013; Cox et al., 2013; Hajima et al., 2014). Based on these studies, there is today an emerging consensus regarding the relative amplitude of those two opposing feedbacks, and that the land and the ocean will continue to absorb an important fraction of the anthropogenic carbon emissions in the near future (Ciais et al., 2013; Figure 2). However, the

Earth carbon uptake capacity is also likely to diminish and, eventually, to saturate (Anav et al., 2013; Arora et al., 2013), not only due to the climate impacts on biomass production and on soil respiration (Friedlingstein et al., 2006), but also because of the natural constraints on NPP (e.g., nutrient limitations; Goll et al., 2012). However, there are still very large uncertainties in the amplitude these effects as controlled by the terrestrial biosphere (Arora et al., 2013; Ciais et al., 2013; see Figure 2).

The use of observational benchmarks emerges as a useful way to constrain some of these uncertainties. Cox et al. (2013) recently reported a strong correlation between the long-term response of land carbon storage to warming in the tropics, and the observed interannual co-variability of atmospheric CO_2 growth and temperature. This study indicates an overestimation of carbon-climate feedback in C4MIP models (Figure 3).

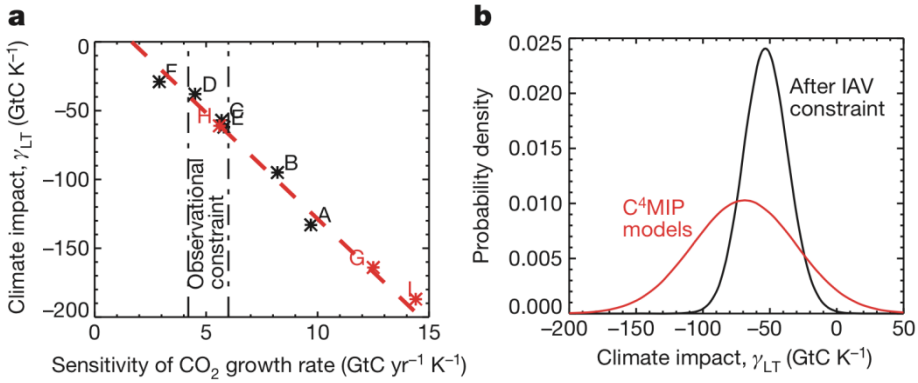

Figure 3: Emergent constraint on the sensitivity of tropical land carbon to climate change. (a) Climate sensitivity of tropical land carbon (γ_{LT}) versus the sensitivity of the CO_2 growth rate to tropical temperature, for each of the models shown in Table 1. The dashed line shows the best-fit straight line across the C4MIP models (black). The red symbols represent a test of this relationship against the three HadCM3C ensemble members. The dot–dash lines indicate the constraint on the observed interannual variability (IAV) in the CO_2 growth rate derived from Figure 2b. (b) PDF for the climate sensitivity of γ_{LT}. The black line was derived by applying the IAV constraint to the across-model relationship shown in a. The red line shows the 'prior' PDF that arises from assuming that all of the C4MIP models are equally likely to be correct and that they come from a Gaussian distribution. From Cox et al., 2013.

Besides the studies focused on the carbon cycle and climate interactions, the direct effects of elevated atmospheric CO_2 on plant physiology and structure (greening), and the resulting impacts on climate, have been explored with models (either ESMs or LSMs) since the late 1990s. Betts et al. (1997) reported opposite effects on the global climate (temperature and precipitation) of similar amplitude driven by the physiological reduction of transpiration, on one hand, and by leaf area index (LAI) increases on the other. Yet, the combined impacts of these two mechanisms lead to a net reduction in Amazonian evapotranspiration (ET). Levis et al. (2000), found an even larger offsetting effects of CO_2 (physiological versus structural) on

the surface hydrology due to an expansion of forest and large increases in LAI.

Based on forced LSM simulations, Gedney et al. (2006) attributed the historical trends in global runoff (positive) to the CO_2-physiological reduction in transpiration and ET. This result was confronted by Piao et al. (2007), showing little direct impacts of CO_2 on runoff. In this case, the historical runoff trends were mainly associated with climate variability (precipitation principally) and LULCC. The weak direct impacts of CO_2 on global runoff found by Piao et al. (2007) were in part the result of offsetting physiological (reduction) and structural (increases) effects on canopy transpiration. A similar conclusion was reported for the historical period by Alkama et al. (2010) and Peng et al. (2013).

Regarding the future projections, Kergoat et al. (2002) reported a weak net (physiological and structural) ET response to doubled CO_2, echoing the results of Betts et al. (1997) and Levis et al. (2000). In turn, Betts et al. (2007), Alkama et al. (2010) and Gopalakrishnan et al. (2011) found an important contribution of CO_2-driven reduction in transpiration to future increase in global runoff.

3 Radiative and physiological impacts of CO_2 in Amazonia

3.1 Model data and methods

In this section, we present analyses of three idealized and complementary modelling experiments, designed within the CMIP5 framework to evaluate the climate sensitivity to the increase in atmospheric CO_2 concentration (hereafter ΔCO_2) and the climate-carbon cycle feedbacks (Taylor et al., 2012). The focus is on the Amazon basin climate and carbon balance and, rather than assessing feedback strengths, we look at the amplitude and uncertainties of the radiative and biochemical effects of ΔCO_2.

Following the CMIP5 nomenclature, the three modelling experiments analysed are:

- *1pctCO₂*: Transient simulation of at least 140 years initialized from preindustral control runs. The atmospheric CO_2 concentration is prescribed and follows a rising pathway of 1% per year. All other natural (e.g., volcanic activity) and anthropogenic (e.g., LUC) climate forcings are avoided. The ESMs schemes include both the radiative and biochemical effects of CO_2.
- *esmFixClim1*: Similar to *1pct*CO_2, but the radiative response to ΔCO_2 is disabled in the ESMs. This experiment thus isolates the physiological effects of ΔCO_2 (e.g., plant

fertilization) and the associated environmental impacts.

- *esmFdbk1*: Similar to *1pct*CO_2, but with the biochemical response to ΔCO_2 disabled. Then, the ESMs see only the physical (radiative) effects of ΔCO_2 (e.g., large-scale warming).

These simulations were carried out by a subset of ESMs participating in CMIP5. In this report we use the outputs of eight ESMs, for which the three types of simulations described above were available. These models and some basic configurations of them are listed in Table 1. An in-depth description of these models and other ESMs assessed in CMIP5 can be found in Arora et al. (2013) and Flato et al. (2013).

In this report, RAD and BGC refer to the radiative and biogeochemical response of the climate system to ΔCO_2 that is derived from simulations *esmFdbk1* and *esmFixClim1*, respectively. We use ALL to denote the coupled radiative-biochemical effects deduced from *1pctCO₂*. The synergies between both effects are also evaluated by comparing ALL to the diagnosed net effect of ΔCO_2 derived from RAD+BGC.

All the model outputs were interpolated to a common grid of 1.0 latitude-longitude. The model response to ΔCO_2 is quantified either as the evolution of a given variable across the whole 140-yr period or as the difference between the last and first 30 years of this period. We also refer to the preindustrial (PI) mean as climatologies computed over the first 30 years. We note that the atmospheric CO_2 increases by a factor 3 between two time windows used here (Figure 4).

After 140 years, the ensemble of simulations RAD indicates a warming of around 5.0 ± 1.2 K on average over the continents (Figure 4). The biochemical effect of ΔCO_2 amplifies this impact by 0.5 ± 0.5 K — a behaviour likely caused by reductions in land ET (see Section 3.3).

Table 1. CMIP5 coupled climate-carbon cycle models (ESMs) used this study.

ESM ref. number & acronym	Modelling group	Land surface model	Dyn. veget.	N cycle	Reference
(1) bcc-csm1.1	BCC, China	BCC_AVIM1.0	no	no	Xin et al. (2013)
(2) CanESM2	CCCMA, Canada	CLASS2.7-CTEM1	no	no	Arora et al. (2011)
(3) CESM-BGC	NSF–DOE–NCAR, USA	CLM4	no	yes	Long et al. (2013)
(4) GFDL-ESM2M	NOAA-GFDL, USA	LM3	yes	no	Dunne et al. (2013)
(5) HadGEM2-ES	MOHC, UK	JULES-TRIFFID	yes	no	Collins et al. (2011)
(6) IPSL-CM5A-LR	IPSL, France	ORCHIDEE	no	no	Dufresne et al. (2013)
(7) MPI-ESM-LR	MPI-M, Germany	JSBACH-BETHY	yes	no	Giorgetta et al. (2013)
(8) NorESM-ME	NCC, Norway	CLM4	no	yes	Tjiputra et al. (2013)

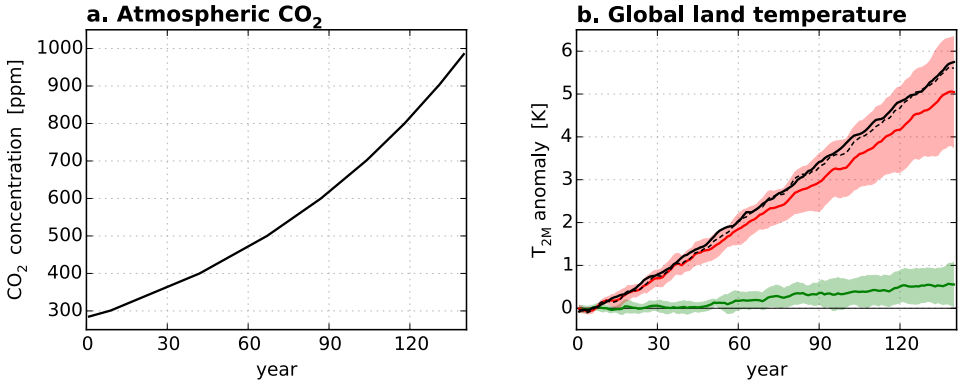

Figure 4: (a) Atmospheric CO_2 concentration prescribed in simulations *esmFdbk1* (RAD), *esmFixClim1* (BGC) and *1pctCO2* (ALL), and (b) modelled mean near-surface temperature over the continents. Thick curves (shading) indicate the model mean (±1.0 std) from simulations RAD (red), BGC (green) and ALL (solid-black). Dashed curve indicates the sum of RAD and BGC.

3.2 Changes in biomass productivity, vegetation carbon and structure

The global distribution of the CO_2-induced changes in NPP is shown in Figure 5. The fertilization effect of CO_2 and associated increase in biomass production is a strong and robust feature in ESMs both in simulations BGC and ALL. Although the direction of this effect is systematic across the models, the amplitude varies widely. In simulation BGC, the models show an increase in global NPP of 33 ± 22 Pg C yr^{-1} between the first and the last 30 years of simulation, which represents an increase above 50% relative to the PI mean NPP (Table 2).

In contrast, the RAD simulations show decreases in the global NPP by around 3.5 Pg C yr^{-1} in response to ΔCO_2 (Table 2). Compared with BGC, in RAD the changes in NPP are more localized in the Tropics, particularly in Amazonia (Figure 5b). Across the basin, the physiological (+3.8 Pg C yr^{-1}; Table 2) and the radiative (−1.4 Pg C yr^{-1}) effects on NPP are of comparable magnitudes (Figure 7a) and, relative to BGC, RAD produces a damping effect of ~35%.

The fertilization effect of CO_2 leads to an increase in vegetation carbon (Table 2) and to a greening that clearly dominate the combined impacts (ALL) across the vegetated lands (Figure 6). Within the Amazon basin, the models simulate a particularly large increase in AGB (+37 ± 18 Pg C in BGC), which explains around 13% the global change in AGB (Table 2). As is the case for NPP, the Amazon rainforest plays a major role in the global AGB disturbance in the RAD simulations. The radiative-driven decrease in Amazonian AGB (15 ± 6 Pg C) explains about 40% of the global RAD impact on this variable (Table 2).

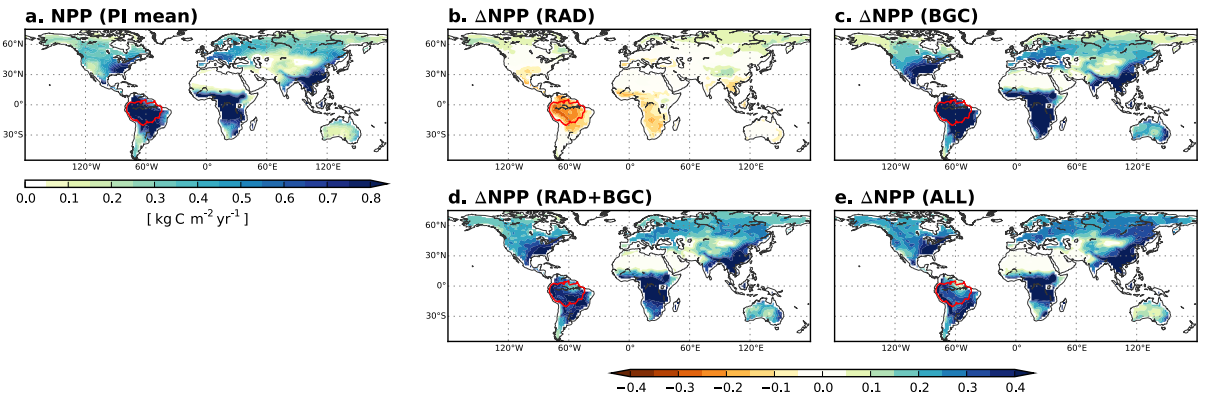

Figure 5: (a) Preindustrial annual mean net primary production (NPP) and (b-e) difference in NPP between the last and first 30 years of simulation (~3×CO_2). Panels (b) and (c) show respectively the radiative (RAD) and biochemical (BGC) response to ΔCO_2. (d) Sum of RAD and BGC and (e) simulated (coupled) response including both effects (ALL). Red contour indicate the Amazon basin domain used in this report.

Table 2. Simulated carbon fluxes (NPP, R_H) and stock in vegetation (AGB) integrated over the global lands and over the Amazon basin. Preindustral (PI) model-mean values and ΔCO_2-induced changes are indicated for the various types of simulations. Values in brackets indicate the inter-model dispersion (1.0 std).

	Global land					Amazonia				
	PI mean	BGC	RAD	BGC+ RAD	ALL	PI mean	BGC	RAD	BGC+ RAD	ALL
NPP [Pg C yr^{-1}]	54 (16)	+33.1 (22.2)	−3.4 (2.6)	+29.7 (20.8)	+29.9 (18.1)	6.6 (2.5)	+3.8 (2.9)	−1.4 (0.9)	+2.5 (2.1)	+2.2 (1.7)
R_H [Pg C yr^{-1}]	51 (9)	+26.1 (16.7)	−1.2 (1.6)	+24.9 (16.3)	+25.9 (14.1)	6.1 (2.2)	+3.3 (2.7)	−0.9 (0.7)	+2.3 (2.1)	+2.1 (1.5)
AGB [Pg C]	685 (288)	+290 (121)	−37 (17)	+253 (111)	+267 (114)	83 (36)	+37 (18)	−15 (6)	+22 (17)	+24 (22)

In terms of LAI, the greening effect simulated in BGC and the opposite impacts simulated in RAD are particularly large in Amazonia (above 1.0 m^2 m^{-2} in several cases; Figure 8b). The magnitudes of both effects, on average across the models, are similar and roughly offset each other (Figures 6 and 7c). A synergy between biochemical and radiative processes is also observed in this case; the ALL simulation produces a net LAI increase of larger amplitude that the one deduced from the RAD and BGC simulations separately.

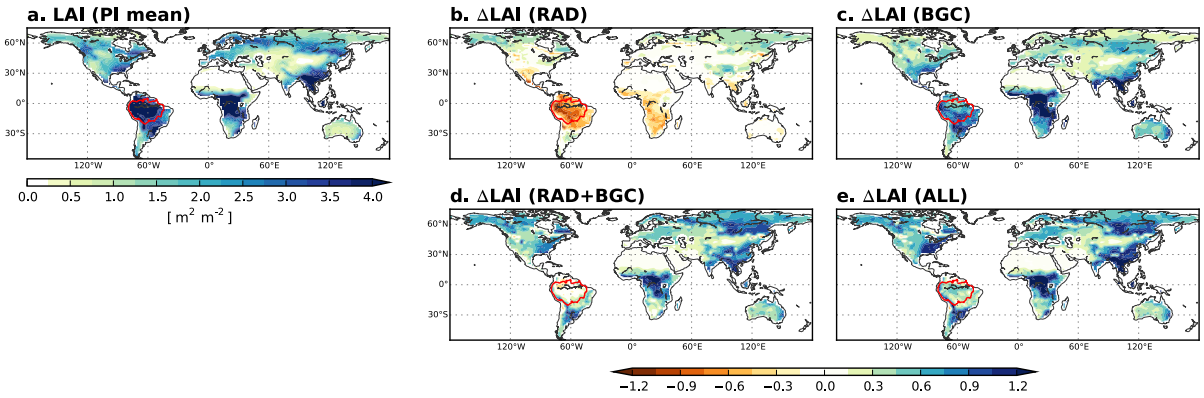

Figure 6: As in Figure 5, but for LAI

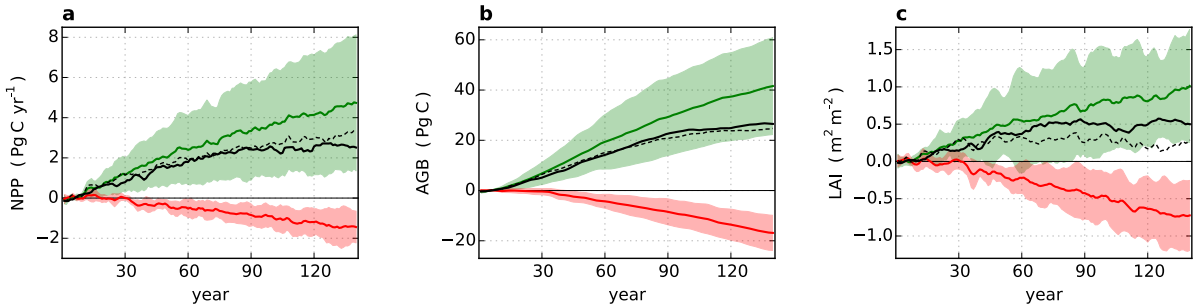

Figure 7: Anomalies of annual (a) net primary production, (b) above-ground biomass and (c) leaf area index simulated on average across the Amazon basin in response to the atmospheric CO_2 1% yr^{-1} increase. Thick lines and shading indicate the multi-model mean ± 1.0 std in BGC (green) and RAD (red) simulations. Solid and dashed black curves show the model-mean anomalies in the coupled radiative-biochemical simulation (ALL) and resulted from the sum of BGC and RAD, respectively.

The individual model responses to ΔCO_2 simulated in RAD and BGC are illustrated in Figure 8. For comparison, the differences in annual AGB between the last and first 30 years of simulations are plotted against the difference in NPP (Figure 8a); the corresponding changes in LAI vs. AGB are also illustrated in Figure 8b. In the first case, a positive correlation between ΔAGB and ΔNPP is observed across the ESMs and across the two modelling experiments. Some clear differences are, however, observed within the models. For instance, HadGEM2-ES (#5) and MPI-ESM-LR (#7) show, for the corresponding change in NPP in BGC simulations, moderate AGB increases compared to the model ensemble. We note that those two models, in addition to GFDL-ESM2M (#4), have their DVGM enabled (Table 1). However, there is no common behaviour between ΔAGB/ΔNPP and vegetation changes in those models. In the BGC simulations, the Amazonian forest area increases in the cases of

GFDL-ESM2M (#4) and HadGEM2-ES (#5), and decreases in MPI-ESM-LR (#7) (not shown).

A more definite correlation is observed between the simulated changes in LAI and AGB (Figure 8b). In this case, there are again some models that do not follow the leading ΔLAI-ΔAGB relationship in BGC simulations. Three ESMs show clearly weaker LAI sensitivities to increases in AGB, and make the model-mean change in this variable of similar amplitude as the mean LAI changes simulated in RAD. A possible cause for this behaviour is that those models have included a maximum LAI threshold in their land-surface parameterizations, hence avoiding their carbon allocation on leafs. This is the case for ORCHIDEE (LSM embedded in IPSL-CM5A-LR, #6), where LAI is limited to a value of 7.0 m^2 m^{-2}. In the cases of bcc-csm1-1 (#1) and MPI-ESM-LR (#7), the suppressed LAI increases may be related to feedbacks with environmental disturbances.

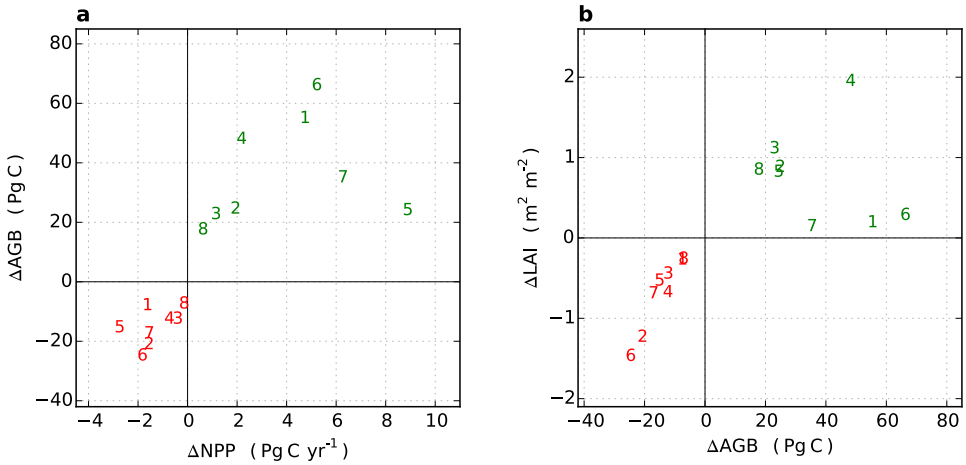

Figure 8: Difference in the Amazon basin mean annual ABG between last and first 30 years of simulation, plotted against the corresponding change in NPP. Numbers indicate the individual model responses to ΔCO_2 (Table 1) in simulations BGC (green) and RAD (red). (b) As in panel (a), but for the changes in LAI vs. changes in AGB.

The ESMs are systematic in simulating an increase in the Amazonian NPP in BGC simulations (Figure 9a). In these simulations, the models also show consistent behaviour in their canopy transpiration (TR) response to ΔCO_2, which decrease in all of them (Figure 9b). This means that in all models, the CO_2-physiological impact on canopy conductance (stomatal closure) and associated TR suppression overwhelms the opposite effect expected from increases in LAI (also systematic within the ESMs; Figure 8b). This model behaviour is of great importance regarding the hydrological impacts of ΔCO_2 (drying) across the Amazon basin (see section that follows), and questions previous findings that indicate weaker CO_2-

physiological impacts on the surface hydrology, precisely because of the competing effects of those two mechanisms (e.g., Kergoat et al., 2002; Piao et al., 2007). We note, however, that the historical CO_2-impact reconstructions — such as the one carried out by Piao et al. — may differ from the ones assessed here because of different levels of perturbation (e.g., the impacts on LAI may saturate at high ΔCO_2 levels).

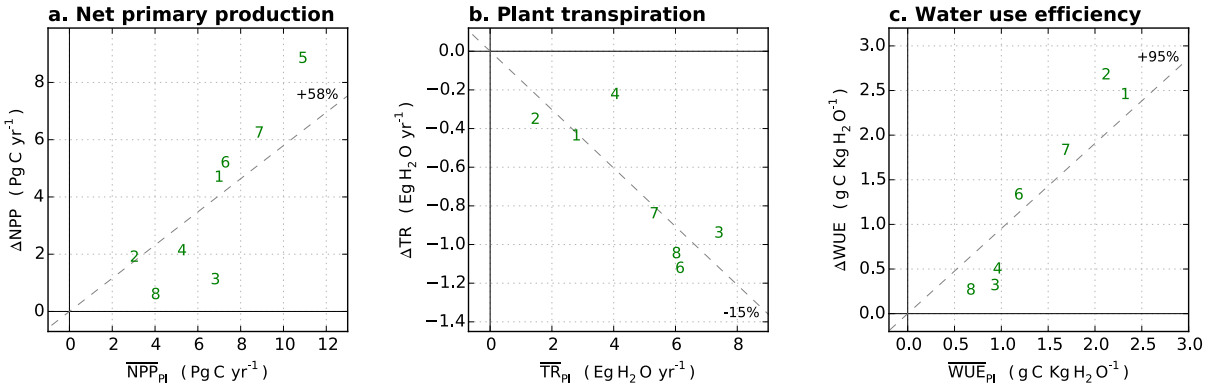

Figure 9: Difference in the Amazon basin mean annual (a) net primary production, (b) plant transpiration and (c) water use efficiency between the last and first 30 years of simulation BGC, plotted against the climatological (preindustrial) mean of the corresponding variable. Numbers indicate the results from the various ESMs (Table 1). Note that there are no transpiration and WUE data for HadGEM2-ES (#5) (not available). Dashed lines show the linear fit computed within the ESM values (without constant term).

Given the systematic and opposite directions of the CO_2-physiological impacts on the Amazonian NPP and TR, all the models simulate an increase in water use efficiency (derived here as the ratio between NPP and TR) in BGC simulations (Figure 9c). The WUE sensitivity to ΔCO_2 is a key parameter to understand the physiological impact uncertainties both in the carbon cycle and in climate. The CMIP5 ESMs indeed show large differences in their NPP, TR and WUE responses to ΔCO_2. The modelled changes in these variables in Amazonia correlate fairly well with the corresponding PI climatologies (Figure 9). Similar behaviour was reported by Anav et al. (2013). Besides this constraint, some model differences are more clearly contrasted. As noted by Arora et al. (2013), the two models accounting for nutrient-limitation (Nitrogen) — those using CLM4 as LSM (#3 and #8, Table 1) — show moderate increases in NPP (Figure 9a).

Compared to the model ensemble, GFDL-ESM2M (#4) simulates in Amazonia a particularly weak decrease in TR with respect to its climatology (Figure 9b). The CO_2 greening effect may explain the dampened physiological forcing on TR in this model, which shows a particularly large LAI increase in the BGC simulation (Figure 8b). For the Amazonian WUE, the climatological constraint appears to be particularly robust across the models (Figure 9c). The WUE increase in BGC simulations follows closely their PI means at a mean rate of 95%. That

is, the models roughly double their WUE in Amazonia in the BGC simulation for a forcing equivalent to ~3×CO_2.

3.3 Changes in climate and hydrological variables

There are several mechanisms that may contribute to regional climate changes in response to ΔCO_2. The impacts on ET, on the water recycling and on precipitation (P) are of particular interest in Amazonia given the vulnerability of the rainforest to changes in the local rainfall regime and to the biophysical feedbacks associated with them. The idealized simulations assessed here serve to clarify some of these processes. The following relations are speculative ways in which ΔCO_2 could perturb the local ET over the continents both through RAD and BGC:

RAD: $+ CO_2 \rightarrow \pm P \rightarrow \pm \theta \rightarrow \pm ET$ (1)

RAD: $+ CO_2 \rightarrow + T_a \rightarrow + VPD \rightarrow + ET$ (2)

RAD: $+ CO_2 \rightarrow + T_a \rightarrow - NPP \rightarrow - LAI \rightarrow - ET$ (3)

BGC: $+ CO_2 \rightarrow - g_s \rightarrow - TR \rightarrow - ET$ (4)

BGC: $+ CO_2 \rightarrow + NPP \rightarrow + LAI \rightarrow + ET$ (5)

The first mechanism makes reference to the RAD-induced changes in P and the concomitant impacts on soil moisture (θ) and ET. The radiative P response to ΔCO_2 results from a combination of thermodynamic and dynamic disturbances in the atmosphere (Bony et al. 2013; Boisier et al., submitted). These are spatially and seasonally dependent, and remain highly uncertain in some regions (notably in Amazonia; Joetzjer et al., 2013). The water-limited regions should, in this case, be more sensitive to changes in P (Seneviratne et al. 2010). Mechanism (2) refers to the increase in ET driven by the enhanced water demand of a warmer atmosphere. Further, RAD could also affect ET thought changes in productivity and in LAI. As described above, the largest radiative effects on LAI are simulated across Amazonia (decreases), an impact that should lead to a relative reduction of ET.

The global distribution of the simulated mean changes in annual ET and P are illustrated in Figures 10 and 11, respectively. The ESMs show in their RAD simulations a prevailing increase in evaporation and P over the oceans — a feature that illustrates the acceleration of the global hydrological cycle expected in a warmer world (Trenberth, 2011). Increases in ET also dominate in high-latitude land regions, probably as a combination of the above-mentioned mechanisms (1) and (2). In tropical lands and across the Amazon basin,

particularly, there is not a clear RAD signal on ET in the multi-model mean.

On the other hand, the BGC simulations show quite a clear ET response to ΔCO_2 in the tropics. A decrease of ET in these regions is likely the result of the reduction in plant stomatal conductance and in transpiration (Figure 9b). As commented above, this mechanism (#4) seems to dominate in Amazonia not only over other possible BGC effects [e.g., mechanism (5)], but also over the impacts driven by RAD (Figs. 10 and 12).

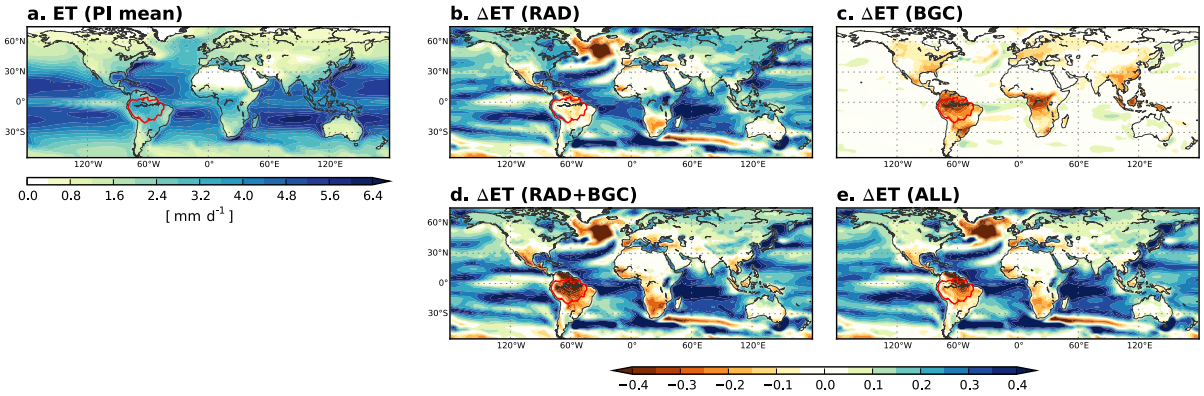

Figure 10: As in Figure 5, but for evapotranspiration (ET).

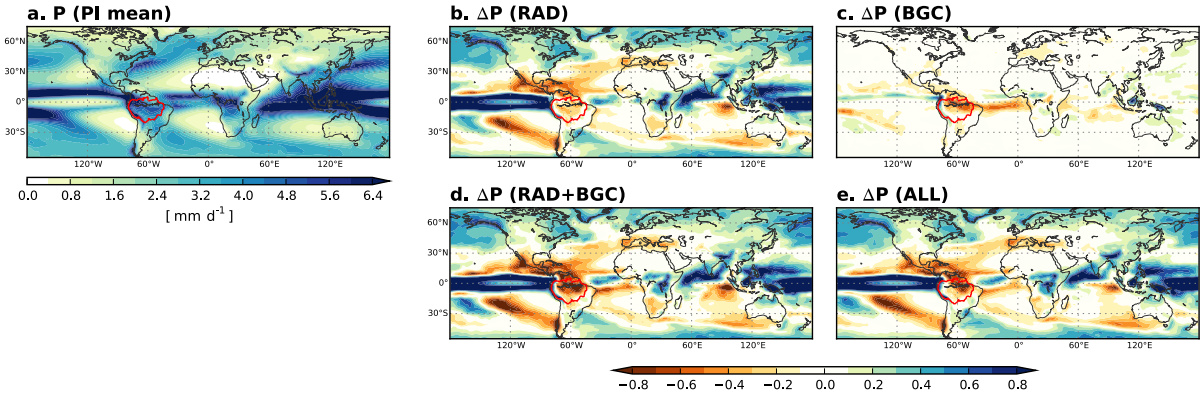

Figure 11: As in Figure 5, but for precipitation (P).

The BGC-driven ET reduction in the tropics is very likely the driving factor for a warmer and drier climate in Amazonia (Figs. 11 and 12). The simulated warming across the Amazon basin in RAD simulations (+4.1 ± 1.4 K) is amplified by 20% when the biochemical processes are included (~+0.8 ± 0.6 K in BGC). The ensemble mean annual precipitation change is negative in both experiments BGC (−0.25 ± 0.21 mm d^{-1}) and RAD (−0.16 ± 0.33 mm d^{-1}), but of weaker signal-to-noise ratio in the latter case. Yet, the amplitude of these impacts is moderate

compared to basin mean annual rainfall totals (~5% in the BGC case).

Table 3: Simulated water fluxes (ET, P and P-ET) integrated over the global lands and over the Amazon basin. Preindustral (PI) model-mean values and ΔCO_2-induced changes are indicated for the various types of simulations. Values in brackets indicate the inter-model dispersion (1.0 std).

	Global land					Amazonia				
	PI mean	BGC	RAD	BGC+ RAD	ALL	PI mean	BGC	RAD	BGC+ RAD	ALL
ET [$km^3\ d^{-1}$]	198 (19)	−11.0 (8.0)	+9.7 (3.7)	−1.3 (4.6)	+0.7 (4.3)	22.2 (3.9)	−2.0 (1.0)	−0.3 (1.2)	−2.3 (1.6)	−1.5 (1.6)
P [$km^3\ d^{-1}$]	281 (28)	−3.9 (6.9)	+14.0 (5.2)	+10.1 (4.1)	+12.1 (5.5)	33.6 (7.3)	−1.8 (1.5)	−1.2 (2.3)	−2.9 (2.9)	−1.8 (3.2)
P − ET [$km^3\ d^{-1}$]	83 (16)	+7.1 (6.4)	+4.3 (3.1)	+11.4 (5.6)	+11.5 (6.2)	11.4 (4.2)	+0.2 (1.2)	−0.9 (1.6)	−0.7 (1.5)	−0.3 (1.8)

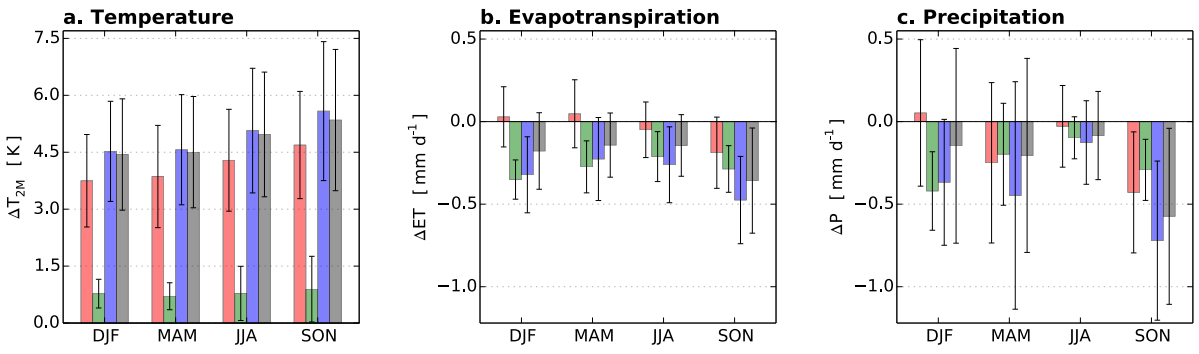

Figure 12: Difference in the Amazon basin mean (a) 2m-temperature, (b) evapotranspiration and (c) precipitation between the last and first 30 years of simulation. Boxes (error bars) indicate the seasonal model mean (± 1.0 std) response to the atmospheric CO_2 increase in RAD (red), BGC (green) simulations. Blue and grey bars show the combined radiative-biochemical effect in the corresponding variable resulted from the sum of BGC and RAD, and simulated in ALL, respectively.

The seasonal detail of the simulated changes in the Amazonian temperature, ET and P is shown in Figure 12. The model-mean temperature and ET responses to ΔCO_2 in BGC are systematic throughout the year. Give the strong rainfall seasonality in Amazonia, the changes in P show more pronounced annual cycle. However, as for ET, the dominant (drying) signal is also present from season to season in BGC simulations. This feature points out the widespread ET decrease (Figure 10c) as a plausible cause of drying in Amazonia through reduced water recycling. The approximate linear inter-model relationship between the annual ΔET and ΔP also suggests this mechanism in BGC simulations (green markers in Figure 13a).

Compared to the CO_2-physiological forcing, the ESM radiative P responses to ΔCO_2 show a weaker signal-to-noise ratio (Figure 12c). There is also a less clear relationship between ΔET and ΔP in this case (red markers in Figure 13a) — a feature expected given the large-scale atmospheric control of the rainfall perturbations in RAD.

The ET and P changes indicate a synergistic effect between the radiative and biochemical impact of ΔCO_2. In both variables, the net impact simulated across the Amazon basin in ALL (model-mean drying) is of weaker amplitude than the one deduced from RAD+BGC (Figure 12). To inquire into the driving factors of this effect, we plotted the differences between changes deduced from RAD+BGC and the ones simulated in ALL in those two variables, against the corresponding differences and LAI (Figure 13b,c). In the two cases, a close inter-model relation is found for six of the eight ESMs, suggesting LAI as the main cause of this behaviour.

We note that the different net impact to ΔCO_2 on LAI in ALL simulations relative to RAD +BGC affects IPSL-CM5A-LR (#6) principally (Figure 13b), model that includes a strong constraint through an imposed maximum LAI threshold. The strong synergistic effect in this model can be understood as follows: the CO_2-induced greening leads to LAI saturation in ORCHIDEE (LSM embedded in the IPSL ESM) and, given the opposite biochemical and radiative effects on LAI (Figure 7b), this saturation occurs later in time and is therefore dampened in ALL compared to BGC, resulting in a net LAI increase of larger amplitude in the former case.

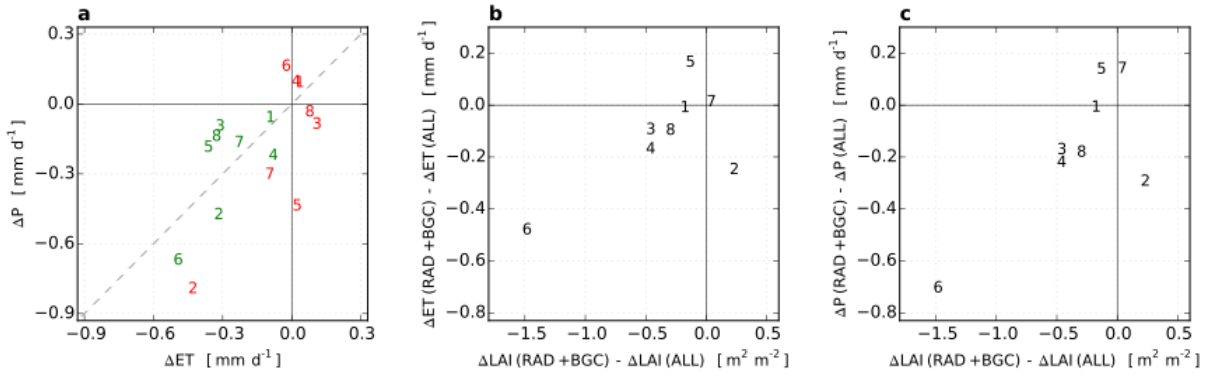

Figure 13: (a) Difference in Amazonian annual precipitation (P) between the last and first 30 years of simulation, plotted against the corresponding difference in evapotranspiration (ET). Numbers indicate the individual ESM responses (Table 1) to CO_2 increases in RAD (red), BGC (green) simulations. (b) Difference between the combined radiative-biochemical impacts of ΔCO_2 on ET calculated with RAD +BGC and simulated in ALL, plotted against the corresponding difference in LAI. (c) As in panel (b), but for P.

3.4 The HadGEM2-ES case study

The response of ET in this model (Figure 14) over Amazonia is in broad agreement with the multi-model means (Figure 10), in that in ALL, there are widespread decreases in ET which are most marked towards the northeast, although the reduction in this region is greater than the multi-model mean. In BGC, HadGEM2-ES exhibits reduction in ET of comparable magnitude to the multi-model mean. In RAD there are regional differences in the sign of the response: ET increases in the western Amazon and decreases in east. This is likely to reflect the regional climate response which shows considerable uncertainty among models, as mentioned in Section 3.3.

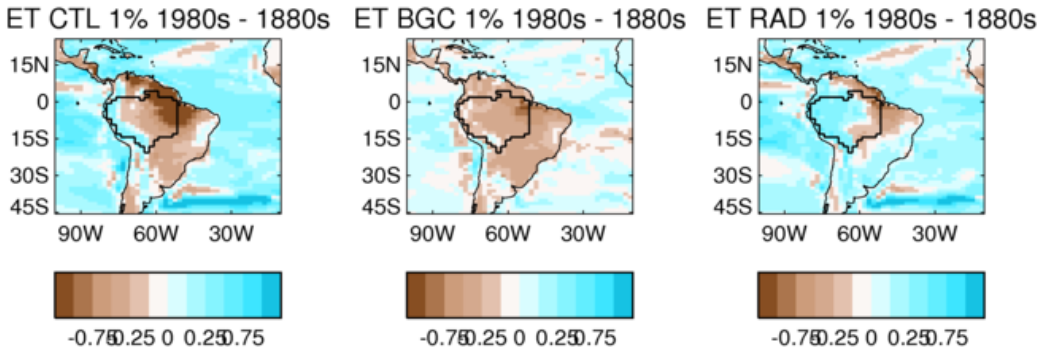

Figure 14: Difference in Amazonian annual evapotranspiration (ET) in mm/day between the last and first 30 years of simulation in HadGEM2-ES in (a) ALL, (b) BGC and (c) RAD simulations. Thick black line indicates outline of Amazon Basin.

The combined response of BGC+RAD (Figure 15b) is less than the response in ALL (Figure 14a), in which radiative and physiological effects are permitted to interact; Figure 15c shows the difference between ALL and BGC+RAD. The response of HadGEM2-ES contrasts with the multi-model means (Figure 10d and e, Table 3), in which the BGC+RAD response is greater than that in ALL. It is shown to be the only one of the 8 ESMs to show this behaviour (Figure 13b). It has not yet been determined whether the ALL response is greater than BGC +RAD in all seasons or on sub-daily timescales, however; the multi-model mean response in annual data is also seen in each of the seasons (Figure 12b).

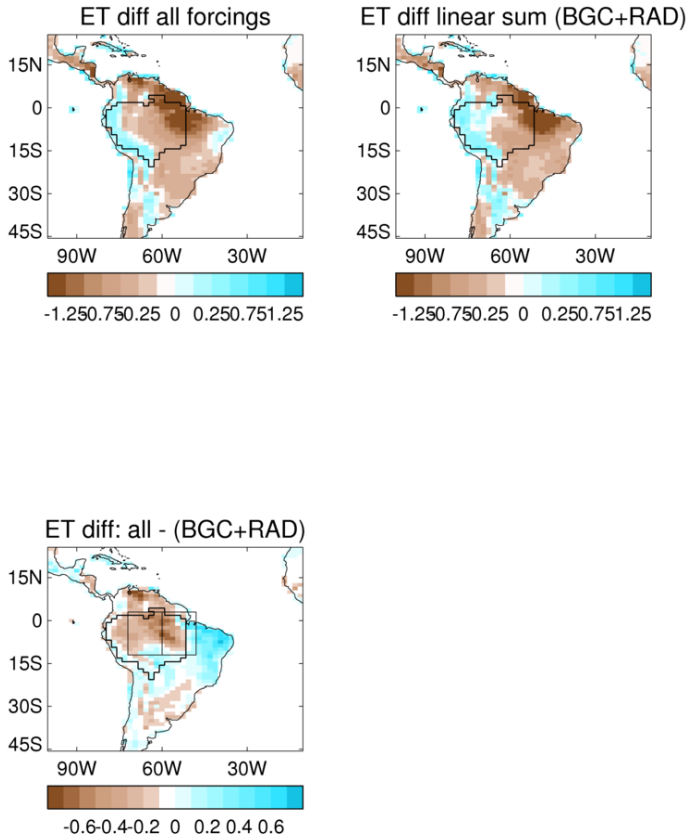

Figure 15: Difference in Amazonian annual evapotranspiration (ET) in mm/day between the last and first 30 years of simulation in HadGEM2-ES in (a) ALL, (b) BGC+RAD and (c) difference between (a) and (b) as a mean over the last 30 years of the simulation. Thick black line indicates outline of Amazon Basin. Thin black lines indicate the east and west Amazon regions based on Malhi et al. (2009b).

Evapotranspiration in HadGEM2-ES is calculated using the following equation (Best et al, 2011):

$$E = \frac{\rho}{r_a + r_s}\left(Q_{sat}(T_*) - Q_1\right) \quad (1)$$

where E is evapotranspiration, ρ is air density, r_a is aerodynamic resistance, r_s is stomatal resistance, $Q_{sat}(T_*)$ is the saturated specific humidity at the surface and Q_1 is the specific humidity at the lowest model level. This equation can be broken down into net resistance $1/(r_a+r_s)$ and moisture $\rho(Q_{sat}(T_*)-Q_1)$ gradient terms. These terms have been examined separately to investigate the behaviour of ET, both in terms of the enhanced ET reductions in ALL compared with BGC+RAD, and the differences between the west and east Amazon in ALL.

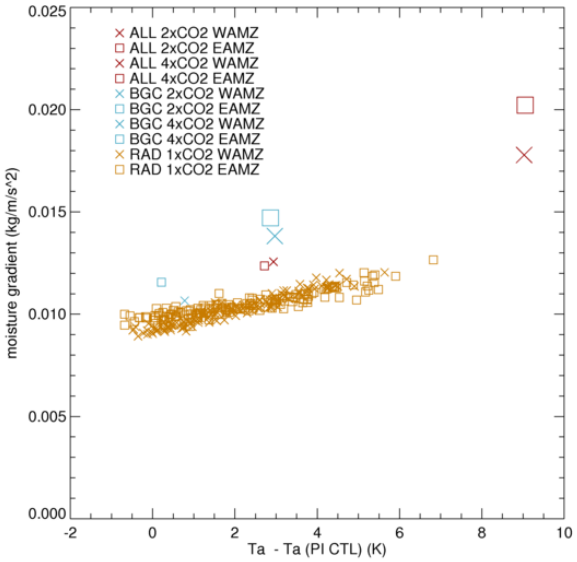

Figure 16: Annual 1.5m temperature change from pre-industrial versus moisture gradient for all points in RAD simulation (atmospheric CO_2 concentration is 1x pre-industrial for vegetation), and points from BGC and ALL simulations at which atmospheric CO_2 concentration is 2× and 4× pre-industrial, averaged over east and west Amazon regions (outlined in Figure 15). Larger squares and crosses indicate 4×CO_2.

The moisture gradient term shows a clear relationship with temperature (Figure 16). In the RAD simulation, the increase in moisture gradient per degree K of temperature rise is the same in the east and west Amazon despite their different climates. An increase in moisture gradient would act to increase ET (through equation 1 and mechanism 2 section 3.3). It is apparent that radiative forcing increases moisture gradient through mechanism 2 in RAD but in BGC the mechanism is less apparent. Although the direct effect on ET is through mechanism 4 and the net resistance term in equation 1, the resultant decrease in ET can modify the boundary layer temperature and humidity so as to increase moisture gradient and ET in a negative feedback. (Seneviratne et al., 2010)

In the BGC and ALL simulations (i.e. with physiological forcing), the increase per K is greater, but there are differences between the west (crosses) and east Amazon (squares). The moisture gradient increase per K in the east Amazon appears very similar in BGC and ALL, suggesting that there is little or no feedback. In the west Amazon it is less steep in ALL than in BGC, which may indicate the presence of a feedback as described above.

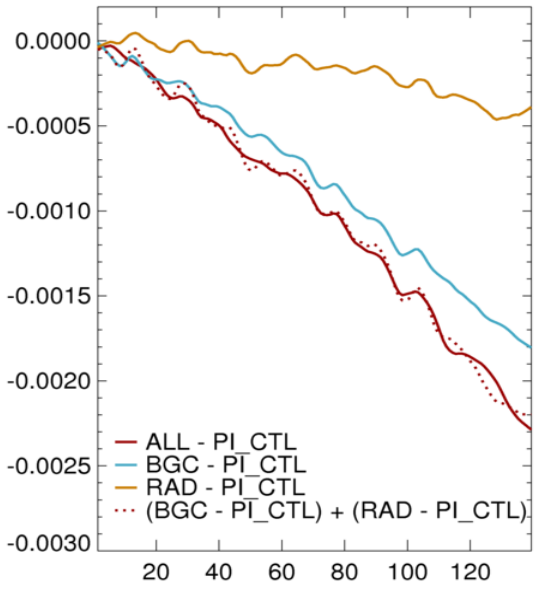

Figure 17: Annual time series of difference from pre-industrial 1/net resistance in sm^{-1} from HadGEM2-ES average over west Amazon in ALL, BGC, RAD and BGC+RAD.

Given that marked decreases in ET occur in both BGC and ALL (Figure 14), despite increases in moisture gradient (Figure 16), it would seem that the net resistance term is dominant in determining ET (mechanism 4 section 3.3). It can be shown that the net resistance is dominated by stomatal resistance, such that fixing aerodynamic resistance at the pre-industrial control value as opposed to using the model values does not affect net resistance. There are marked decreases in 1/net resistance in BGC and ALL; however, this does not explain the difference in ET decrease between ALL and BGC+RAD. The weak decrease in RAD is driven by decreases in soil moisture which is used to scale GPP. The stomatal conductance then adjusts to maintain a constant ratio between GPP and stomatal conductance at a constant CO_2 concentration (Figure 18).

There is still work to do in understanding the enhanced decreases in ET in the ALL simulation compared with BGC+RAD. It is possible that the spatial and temporal aggregation that has been used so far in the analysis may mask effects occurring at shorter timescales. Analysis of monthly and sub-daily time series may also assist in the understanding of the differences between the east and west Amazon.

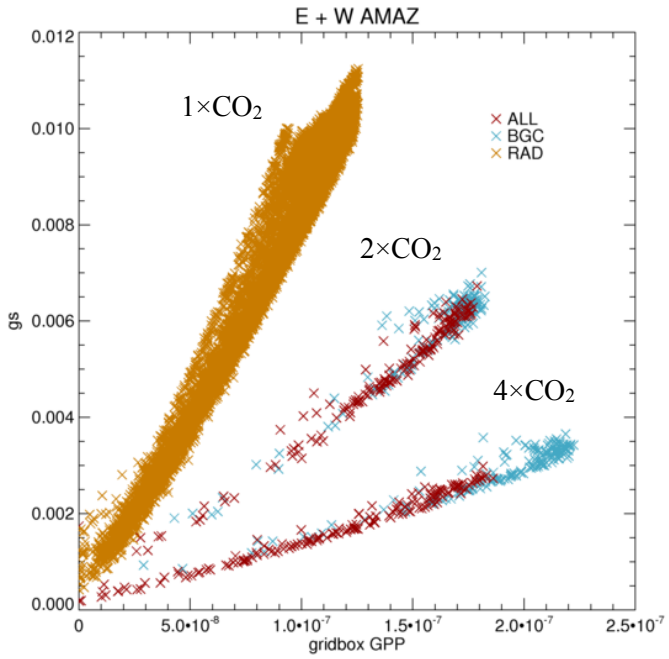

Figure 18: Annual GPP versus stomatal conductance in HadGEM2-ES from 1% simulations with annual timestep from region enclosed by 72°W, 48°W, 12°S, 3°N (east plus west Amazon). All points were taken from RAD simulation. Only points from timestep when CO_2 concentration is 2× and 4× pre-industrial were taken from BGC and ALL as in Figure 16.

4 Concluding remarks

In this report we evaluate the radiative (RAD) and biogeochemical (BGC) effects of CO_2 on the vegetation structure (LAI), on the biomass production/storage, and on the surface climate and hydrology. The results presented are based on an idealized modelling experiment, carried out within CMIP5 by eight ESMs, in which the atmospheric CO_2 concentration increases by 1% per year. Our analyses focus both on the global land areas and on the Amazon basin.

A first result to highlight concerns the relative amplitude of the effects of CO_2 on land carbon sink in BGC and RAD simulations. For a forcing equivalent to around 3×CO_2, the model ensemble indicates a large increase (above 40%) in global vegetation biomass (AGB) in BGC simulations. The change in climate as simulated in RAD dampens the fertilization effect on AGB by near 13% globally (Table 2). In Amazonia, the climate impacts on the land carbon uptake is particularly large; in this region the increase in AGB by fertilization is dampened by 41%. In other words, the contribution of the Amazon rainforest to the global increase in the

global terrestrial carbon sink is reduced from 13% to 9% when the climate (radiative) effects are accounted for.

Another interesting result regards the modelled CO_2-physiological effect on the surface hydrology in Amazonia. On average across the basin, the water use efficiency increases by nearly 100% in BGC simulations between the first and last 30 years of simulation (Figure 9c). This large impact is due to large increases in NPP but also to canopy transpiration reductions (of 15% on average). As a result, the annual mean evapotranspiration (ET) decreases in Amazonia by 9% on average. Probably because of moisture recycling decrease, a drying signal is also observed in BGC simulations. Although moderate, the precipitation reduction in BGC simulations (5%) appears as a more robust response to the CO_2 forcing compared with RAD. Indeed, the magnitudes of both effects cannot be clearly contrasted given the large inter-model spread in the RAD simulations (Figure 12c). An important point that should be underlined here is that the precipitation projections in Amazonia may be significantly underestimated if the models assessed do not account for the physiological effects of CO_2 on vegetation. We note that this is the case for a large number of GCMs currently evaluated in CMIP5 (Flato et al., 2013). This underestimation may be particularly importnat regarding the changes in the dry season length and the potential effects on vegetation (Boisier et al., submitted).

In contrast with earlier results (e.g., Levis et al., 2000; Kergoat et al., 2002; Piao et al., 2007), the general ET reduction in BGC simulations occurs despite the fertilizing effects of CO_2 and associated increase in LAI (a systematic behaviour across the ESMs assessed). We note that overall effects of ΔCO_2 in global runoff — using P minus ET as proxy (Table 3) — is for a significant increase of 12 ± 6 km^3 d^{-1} (+14%), resulting from a runoff increase in both BGC (+9%) and RAD (+5%) simulations. Hence, the physiological impact relative to RAD obtained in this case, is of similar amplitude or even larger than previous studies that pointed out this effect (e.g., Betts et al., 2007).

References

Aguiar, A. P., et al. Set of land-use scenarios for Brazil, linked to implications for policies**.** Deliverable D4.2 for EU-FP7 Project AMAZALERT (Grant Agreement No. 282664) (2014).

Alkama, R., Kageyama, M. & Ramstein, G. Relative contributions of climate change, stomatal closure, and leaf area index changes to 20th and 21st century runoff change: A modelling approach using the Organizing Carbon and Hydrology in Dynamic Ecosystems (ORCHIDEE) land surface model. J. Geophys. Res. 115, D17112 (2010).

Anav, A. et al. Evaluating the Land and Ocean Components of the Global Carbon Cycle in the CMIP5 Earth System Models. J. Climate 26, 6801–6843 (2013).

Arneth, A. et al. Terrestrial biogeochemical feedbacks in the climate system. Nature Geosci 3, 525–532 (2010).

Arora, V. K. et al. Carbon emission limits required to satisfy future representative concentration pathways of greenhouse gases. Geophys. Res. Lett. 38, L05805 (2011).

Arora, V. K. et al. Carbon–Concentration and Carbon–Climate Feedbacks in CMIP5 Earth System Models. J. Climate 26, 5289–5314 (2013).

Best, M. J. et al. The Joint UK Land Environment Simulator (JULES), model description – Part 1: Energy and water fluxes. Geosci. Model Dev. 4, 677–699 (2011).

Betts, R. A. et al. The role of ecosystem-atmosphere interactions in simulated Amazonian precipitation decrease and forest dieback under global climate warming. Theoretical and Applied Climatology 78, (2004).

Betts, R. A. et al. Projected increase in continental runoff due to plant responses to increasing carbon dioxide. Nature 448, 1037–1041 (2007).

Betts, R. A., Cox, P. M., Lee, S. E. & Woodward, F. I. Contrasting physiological and structural vegetation feedbacks in climate change simulations. Nature 387, 796–799 (1997).

Betts, R. A., Malhi, Y. & Roberts, J. T. The future of the Amazon: new perspectives from climate, ecosystem and social sciences. Philos Trans R Soc Lond B Biol Sci 363, 1729–1735 (2008).

Boisier J. P., Ciais P., Guimberteau M., and Ducharne A. Projected strengthening of Amazonian dry season by constrained climate model simulations (submitted to Nature Climate Change).

Bony, S. et al. Robust direct effect of carbon dioxide on tropical circulation and regional precipitation. Nature Geosci 6, 447–451 (2013).

Boulton, C. et al. Exploring uncertainty of Amazon dieback in a perturbed parameter earth system ensemble (in prep.).

Ciais, P., et al. Carbon and Other Biogeochemical Cycles. In: Climate Change 2013: The Physical Science Basis. Contribution of Working Group I to the Fifth Assessment Report of the Intergovernmental Panel on Climate Change [Stocker, T.F., D. Qin, G.-K. Plattner, M. Tignor, S.K. Allen, J. Boschung, A. Nauels, Y. Xia, V. Bex and P.M. Midgley (eds.)]. Cambridge University Press, Cambridge, United Kingdom and New York, NY, USA (2013).

Collins, W. J., et al. Development and evaluation of an Earth-System model HadGEM2. Geosci. Model Dev., 4, 1051–1075 (2011).

Cox, P. M., Betts, R. A., Jones, C. D., Spall, S. A. & Totterdell, I. J. Acceleration of global warming due to carbon-cycle feedbacks in a coupled climate model. Nature 408, 184–187 (2000).

Cox, P. M. et al. Sensitivity of tropical carbon to climate change constrained by carbon dioxide variability. Nature 494, 341–344 (2013).

Cox, P. M. et al. Amazonian forest dieback under climate-carbon cycle projections for the 21st century. Theor Appl Climatol 78, 137–156 (2004).

Dufresne, J.-L., et al. Climate change projections using the IPSL-CM5 Earth System Model: From CMIP3 to CMIP5. Clim. Dyn., doi:10.1007/s00382-012-1636-1 (2013).

Dunne, J. P., et al. GFDL's ESM2 global coupled climate-carbon Earth System Models Part II: Carbon system formulation and baseline simulation characteristics. J. Clim. (2013).

Field, C. B., Behrenfeld, M. J., Randerson, J. T. & Falkowski, P. Primary Production of the Biosphere: Integrating Terrestrial and Oceanic Components. Science 281, 237–240 (1998).

Flato, G., J. et al. Evaluation of Climate Models. In: Climate Change 2013: The Physical Science Basis. Contribution of Working Group I to the Fifth Assess- ment Report of the Intergovernmental Panel on Climate Change [Stocker, T.F., D. Qin, G.-K. Plattner, M. Tignor, S.K. Allen, J. Boschung, A. Nauels, Y. Xia, V. Bex and P.M. Midgley (eds.)]. Cambridge University Press, Cambridge, United Kingdom and New York, NY, USA (2013).

Friedlingstein, P. et al. Climate–Carbon Cycle Feedback Analysis: Results from the C4MIP Model Intercomparison. J. Climate 19, 3337–3353 (2006).

Friedlingstein, P., Dufresne, J.-L., Cox, P. M. & Rayner, P. How positive is the feedback between climate change and the carbon cycle? Tellus B 55, 692–700 (2003).

Friedlingstein, P. et al. Uncertainties in CMIP5 Climate Projections due to Carbon Cycle Feedbacks. J. Climate 27, 511–526 (2013).

Gedney, N. et al. Detection of a direct carbon dioxide effect in continental river runoff records. Nature 439, 835–838 (2006).

Giorgetta, M. A., et al. Climate and carbon cycle changes from 1850 to 2100 in MPI-ESM simulations for the Coupled Model Intercomparison Project phase 5. J. Adv. Model. Earth Syst., 5, 572–597, doi:10.1002/jame.20038 (2013).

Goll, D. S. et al. Nutrient limitation reduces land carbon uptake in simulations with a model of combined carbon, nitrogen and phosphorus cycling. Biogeosciences 9, 3547–3569 (2012).

Gopalakrishnan, R. et al. Sensitivity of terrestrial water and energy budgets to CO2-physiological forcing: an investigation using an offline land model. Environ. Res. Lett. 6, 044013 (2011).

Hajima, T., Tachiiri, K., Ito, A. & Kawamiya, M. Uncertainty of Concentration–Terrestrial Carbon Feedback in Earth System Models*. J. Climate 27, 3425–3445 (2014).

Hashimoto, H. et al. El Niño–Southern Oscillation–induced variability in terrestrial carbon cycling. J. Geophys. Res. 109, D23110 (2004).

Huntingford, C. et al. Simulated resilience of tropical rainforests to CO2-induced climate change. Nature Geosci. 6, 268–273 (2013).

IPCC. Summary for Policymakers. In: Climate Change 2013: The Physical Science Basis. Contribution of Working Group I to the Fifth Assessment Report of the Intergovernmental Panel on Climate Change [Stocker, T.F., D. Qin, G.-K. Plattner, M. Tignor, S.K. Allen, J. Boschung, A. Nauels, Y. Xia, V. Bex and P.M. Midgley (eds.)]. Cambridge University Press, Cambridge, United Kingdom and New York, NY, USA (2013).

Joetzjer, E., Douville, H., Delire, C. & Ciais, P. Present-day and future Amazonian precipitation in global climate models: CMIP5 versus CMIP3. Clim. Dyn. 41, 2921–2936 (2013).

Jones, C. D., Cox, P. & Huntingford, C. Uncertainty in climate–carbon-cycle projections associated with the sensitivity of soil respiration to temperature. Tellus B 55, 642–648 (2003).

Kay G., et al. Report on estimated likelihood for irreversible collapse. Deliverable D3.4 for EU-FP7 Project AMAZALERT (Grant Agreement No. 282664) (2014).

Kergoat, L. et al. Impact of doubled CO2 on global-scale leaf area index and evapotranspiration: Conflicting stomatal conductance and LAI responses. J.-Geophys.-Res. 107, 4808 (2002).

Le Quéré, C. et al. Global carbon budget 2014. Earth System Science Data Discussions 7, 521–610 (2014).

Lenton, T.M. Early warning of climate tipping points. Nature Climate Change 1, 201–209. doi: 10.1038/nclimate1143 (2011).

Levis, S., Foley, J. A. & Pollard, D. Large-Scale Vegetation Feedbacks on a Doubled CO2 Climate. J. Climate 13, 1313–1325 (2000).

Long, M. C., K. Lindsay, S. Peacock, J. K. Moore, and S. C. Doney. Twentieth-century oceanic carbon uptake and storage in CESM1(BGC). J. Climate, 26, 6775–6800 (2013).

MacDougall, A. H., C. A. Avis, and A. J. Weaver. Significant contribution to climate warming from the permafrost carbon feedback. Nat. Geosci., 5, 719–721, doi:10.1038/ ngeo1573 (2012).

Malhi, Y. et al. Climate Change, Deforestation, and the Fate of the Amazon. Science 319, 169–172 (2008).

Malhi, Y., Saatchi, S., Girardin, C.A.J., Aragão, L.E.O.C. The production, storage and flow of carbon in Amazonian forests, in Amazonia and Global Change, Geophysical Monographs Series 186, doi: 10.1029/2008GM000779 (2009a).

Malhi, Y. et al. Exploring the likelihood and mechanism of a climate-change-induced dieback of the Amazon rainforest. Proc. Natl. Acad. Sci. USA 106, 20610-20615 (2009b).

Marengo, J. et al. Global Warming and Climate Change in Amazonia: Climate-Vegetation Feedback and Impacts on Water Resources. In Amazonia and Global Change (eds. Keller, M., Bustamante, M., Gash, J. & Dias, P. S.) 273–292 (American Geophysical Union, 2009).

Nepstad, D. C., Stickler, C. M., Filho, B. S.- & Merry, F. Interactions among Amazon land use, forests and climate: prospects for a near-term forest tipping point. Philos Trans R Soc Lond B Biol Sci 363, 1737–1746 (2008).

Peng, J. et al. Effects of increased CO2 on land water balance from 1850 to 1989. Theor Appl Climatol 111, 483–495 (2013).

Piao, S. et al. Changes in climate and land use have a larger direct impact than rising CO2 on global river runoff trends. PNAS 104, 15242–15247 (2007).

Saatchi, S. S., Houghton, R. A., Dos Santos Alvalá, R. C., Soares, J. V. & Yu, Y. Distribution of aboveground live biomass in the Amazon basin. Global Change Biology 13, 816–837 (2007).

Schuur, E. A. G. et al. The effect of permafrost thaw on old carbon release and net carbon exchange from tundra. Nature 459, 556–559 (2009).

Seneviratne, S. I. et al. Investigating soil moisture–climate interactions in a changing climate: A review. Earth-Science Reviews 99, 125–161 (2010).

Taylor, K. E., Stouffer, R. J. & Meehl, G. A. An Overview of CMIP5 and the Experiment Design. Bull. Amer. Meteor. Soc. 93, 485–498 (2012).

Tejada-Pinell, G. et al. Review paper on Amazon ecosystem functions and services and their drivers of change. Deliverable D1.4 for EU-FP7 Project AMAZALERT (Grant Agreement No. 282664) (2012).

Tjiputra, J. F., et al. Evaluation of the carbon cycle components in the Norwegian Earth System Model (NorESM). Geophys. Model Dev., 6, 301–325 (2013).

Trenberth K. E. Changes in precipitation with climate change. Clim Res (2011).

Xin, X., L. Zhang, J. Zhang, T. Wu, and Y. Fang. Climate change projections over East Asia with BCC_CSM1.1 climate model under RCP scenarios. J. Meteorol. Soc. Jpn., 91, 413–429 (2013).